Inductively Driven, 3D Liner Compression of a Magnetized Plasma to Megabar Energy Densities

Final Technical Report

Period Covered: August 2009 – August 2014

February 2015

John Slough

MSNW LLC
8551 1543th Avenue NE
Redmond, WA 98052

PREPARED FOR THE U.S. DEPARTMENT OF ENERGY
OFFICE OF FUSION ENERGY SCIENCES
UNDER CONTRACT NO. DE-SC0001247

Executive Summary

To take advantage of the smaller scale, higher density regime of fusion an efficient method for achieving the compressional heating required to reach fusion gain conditions must be found. What is proposed is a more flexible metallic liner compression scheme that minimizes the kinetic energy required to reach fusion. It is believed that it is possible to accomplish this at sub-megajoule energies. This however will require operation at very small scale. To have a realistic hope of inexpensive, repetitive operation, it is essential to have the liner kinetic energy under a megajoule which allows for the survivability of the vacuum and power systems. At small scale the implosion speed must be reasonably fast to maintain the magnetized plasma (FRC) equilibrium during compression. For limited liner kinetic energy, it becomes clear that the thinnest liner imploded to the smallest radius consistent with the requirements for FRC equilibrium lifetime is desired. The proposed work is directed toward accomplishing this goal. Typically an axial (Z) current is employed for liner compression. There are however several advantages to using a θ-pinch coil. With the θ-pinch the liner currents are inductively driven which greatly simplifies the apparatus and vacuum system, and avoids difficulties with the post implosion vacuum integrity. With fractional flux leakage, the foil liner automatically provides for the seed axial compression field. To achieve it with optimal switching techniques, and at an accelerated pace however will require additional funding. This extra expense is well justified as the compression technique that will be enabled by this funding is unique in the ability to implode individual segments of the liner at different times. This is highly advantageous as the liner can be imploded in a manner that maximizes the energy transfer to the FRC. Production of shaped liner implosions for additional axial compression can thus be readily accomplished with the modified power modules. The additional energy and switching capability proposed will thus provide for optimal utilization of the liner energy.

The following tasks were outlined for the three year effort: (1) Design and assemble the foil liner compression test structure and chamber including the compression bank and test foils [Year 1]. (2) Perform foil liner compression experiments and obtain performance data over a range on liner dimensions and bank parameters [Year 2]. (3) Carry out compression experiments of the FRC plasma to Megagauss fields and measure key fusion parameters [Year 3]. (4) Develop numerical codes and analyze experimental results, and determine the physics and scaling for future work [Year 1-3]. The principle task of the project was to design and assemble the foil liner FRC formation chamber, the full compression test structure and chamber including the compression bank. This task was completed successfully. The second task was to test foils in the test facility constructed in year one and characterize the performance obtained from liner compression. These experimental measurements were then compared with analytical predictions, and numerical code results. The liner testing was completed and compared with both the analytical results as well as the code work performed with the 3D structural dynamics package of ANSYS Metaphysics®. This code is capable of modeling the dynamic behavior of materials well into the non-linear regime (e.g. a bullet hit plate glass). The liner dynamic behavior was found to be remarkably close to that predicted by the 3D structural dynamics results.

Incorporating a code that can also include the magnetics and plasma physics has also made significant progress at the UW. The remaining test bed construction and assembly task is was completed, and the FRC formation and merging experiments were carried out as planned. The liner compression of the FRC to Megagauss fields was not performed due to not obtaining a sufficiently long lived FRC during the final year of the grant. Modifications planned to correct this deficiency included a larger FRC source as well as a much larger liner driver energy storage system. Due to discontinuation of the grant neither of these improvements were carried out.

I. INTRODUCTION

The possibility of thermal insulation with a magnetic field forms the basis for Magnetic Fusion Energy (MFE) concepts like the tokamak, but relatively little has been done to explore the possible benefits of a magnetic field for Inertial Fusion Energy (IFE) approaches. The theoretical advantage of magnetic insulation is that fusion gain can be achieved with lower input energy and power. The presence of a large magnetic field in the target substantially suppresses the thermal transport, and thus lowers the imploding power needed to compress the target to fusion conditions. With more time before the target plasma thermal energy is dissipated, a much more massive confining shell can be employed for direct compression, with the dwell time of the confining (metal) shell now providing for a much longer fusion burn time. This thin shell or "liner" does not need to be propelled inward by ablation but can be driven by explosives or even magnetic fields. Additionally, it was found that if the imploding liner could be made to converge in a fully three dimensional manner on to the magnetized target, fusion gain could be achieved on a small scale with sub-megajoule liner (shell) kinetic energy.[1] Another significant theoretical result was obtained by Basko et al.[2] who showed that for a sufficiently magnetized target plasma, fusion ignition would occur even when the usual criteria for IFE fusion gain, that $\rho \cdot R > 0.1$ g/cm^2, was far from being met. Ignition was now possible as long as the magnetic field-radius product, $B \cdot R > 60$ T-cm. Thus fusion ignition could be obtained for MIF targets with much lower compression than required for purely inertial compression.

Magnetic fields can be introduced in a target by conventional coils before compression with the generation of fields by flux compression in the electrically conducting plasma. This is the principle of Magneto-Inertial Fusion (MIF). To achieve sufficient fusion yield on the short inertial timescale for compression (a few microseconds at most), the plasma energy density, while orders of magnitude less than the traditional regime of IFE, must be still quite high (~10^{11} J/m^3). In this Magnetized High Energy Density (MHED) plasma regime required for fusion gain and ignition, the plasma pressure is typically as large as, or larger than the magnetic pressure, and the role of collisions is much stronger than in MFE.

The most straightforward way to obtain the MHED fusion plasma state is to induce a rapid flux compression of a magnetized plasma. The flux compression can be driven by an imploding metal liner, converging plasma jets, or other means. While there are many possible magnetic configurations for the target plasma, important differences in the properties of the MHED plasma equilibrium, stability, and energy transport will dictate which ones make good candidates for fusion. It is believed by the authors and others[3,4] that the simplest and most energetically efficient method for producing an MHED plasma at Megabar energy densities is by the 3D implosion of a metal shell onto a high β Field Reversed Configuration (FRC) target. The approach to be described here is unique in that a very large compression ratio is achieved by employing several thin foil liners, initially at

large radius, that are inductively driven both radially and axially inward to converge at small radius (see Fig. 1).

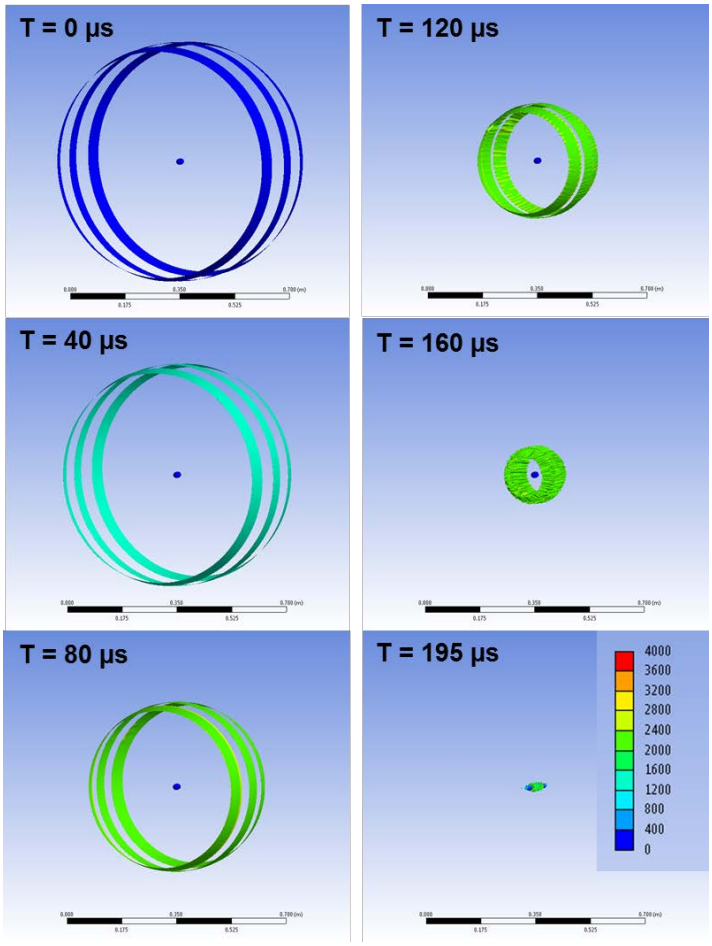

Fig. 1. ANSYS Multiphysics® calculation of the 3D behavior of three 40 cm radius, 5 cm wide, 0.2 mm thick Aluminum liners converging onto a stationary test target. The scale of the ellipsoid target (1×3.5 cm) is that anticipated for an initially 20 cm radius FRC compressed to 1 megabar energy density. Color scale indicates liner velocity.

As will be discussed, an FRC is well suited as the target plasma for compression. The FRC has already demonstrated the confinement scaling at the size and density[5,6] that is required to assure sufficient plasma retention of the target plasma throughout the compression duration required for liner convergence. The FRC naturally has a high β equilibrium and contracts axially with compression thereby considerably simplifying technological requirements for the 3D compression. When generated by FRC merging, the FRC plasmoid can be readily formed inside the converging liner at the appropriate scale by remote FRC generation coils. This makes the FRC the ideal target plasma for the largest possible compression ratio without exceeding optimal plasma temperatures for D-T fusion at maximum compression ($T_i \sim T_e \leq 15$ keV). Thus the target plasma for the Inductively Driven Liner Compression (IDLC) concept presented here is an FRC. It can be generated

by merging FRCs as was first demonstrated at MSNW[7,8] and subsequently at Tri Alpha Energy at even larger scale[9], or it can be generated using a Rotating Magnetic Field (RMF) that can be produced by antenna coils external to the reactor chamber.[10] This technique can be quite advantageous for certain applications as it eliminates the need for any significant ports or penetrations into the reactor.

II. IDLC FUSION CONCEPT DESCRIPTION

Given that fusion ignition conditions are achievable at small scale by applying the kinetic energy of a significantly more massive metal shell to compress the target plasma, the challenge then becomes how to accomplish this. Specifically: can this be done with high driver efficiency, and can it be performed in a manner that is repeatable and that minimizes collateral damage. In addition there is the further challenge of how to create and introduce a suitable magnetized plasma target. The key to solving all these challenges is by employing a process that utilizes these metal shells to not only achieve fusion conditions, but to then act as a buffer for absorbing both neutron and fusion plasma energy. With sufficient fusion gain this shell will be vaporized and ionized in this process. The expanding plasma shell kinetic energy can then be exploited for direct conversion into electricity, or alternatively, it can be used as a high velocity propellant by passage into a magnetic nozzle for directed thrust. A fusion driven rocket employing this highly efficient, direct method for producing high jet power would enable a host of rapid, manned interplanetary missions.[11]

The two most critical issues in meeting these challenges for MIF, and all ICF concepts for that matter, is driver efficiency and “stand-off” – the ability to isolate and protect fusion and thruster from the resultant fusion energy. By employing metal shells for compression, it is possible to produce the desired convergent motion inductively by inserting the metal sheets along the inner surface of cylindrical or conically tapered coils. Both stand-off and energy efficiency issues are solved by this arrangement. The metal shell can be positioned a meter or more from the target implosion site with the coil driver both physically and electrically isolated from the shell. The driver efficiency can be quite high as the coil driver is typically the inductive element of a simple oscillating circuit where resistive circuit losses are a small fraction of the energy transferred. With an in-line element as rudimentary as a diode array, any magnetic energy not imparted to the liner can be recovered back into the charging system after the shell is driven off with the first half cycle. The feasibility of rapidly accelerating inward and compressing thin hoops of aluminum and copper in this manner was first demonstrated by Cnare[12]. Since then, the technique has been employed in several experiments to obtain very high magnetic fields as is envisioned here. Even though there is essentially no magnetic field within the hoops initially, there is enough flux leakage during the inward acceleration that at peak compression the axial magnetic field that is trapped inside the now greatly thickened wall can reach as high as 600 T.[13] As will be seen, a magnetic field of this magnitude is considerably higher than required for compression of the FRC to have ignition and substantial fusion gain.

The next challenge to be considered is the production of the magnetized plasma to be used as the fusion target. As mentioned, it is of paramount advantage to employ a closed field line plasma like the FRC, that has intrinsically high β (plasma/magnetic pressure ratio), and that can be readily translated and compressed for the primary target plasma for IDLC. In addition, the FRC must be of sufficient size to assure sufficient lifetime to survive the compression timescale required for liner-based inertial fusion. In addition the FRC must be formed with enough internal flux to satisfy the B·R ignition criteria at peak compression. At a nominal liner converging speed of 3 km/s, a 0.2 m radius FRC, typical of operation on the LSX FRC device, would be fully compressed in 67 μs which is only a fraction of the lifetime that was observed for these FRCs (~ 1 ms).[6] These FRCs also had more than sufficient internal flux to satisfy the magnetic ignition criterion at full compression.

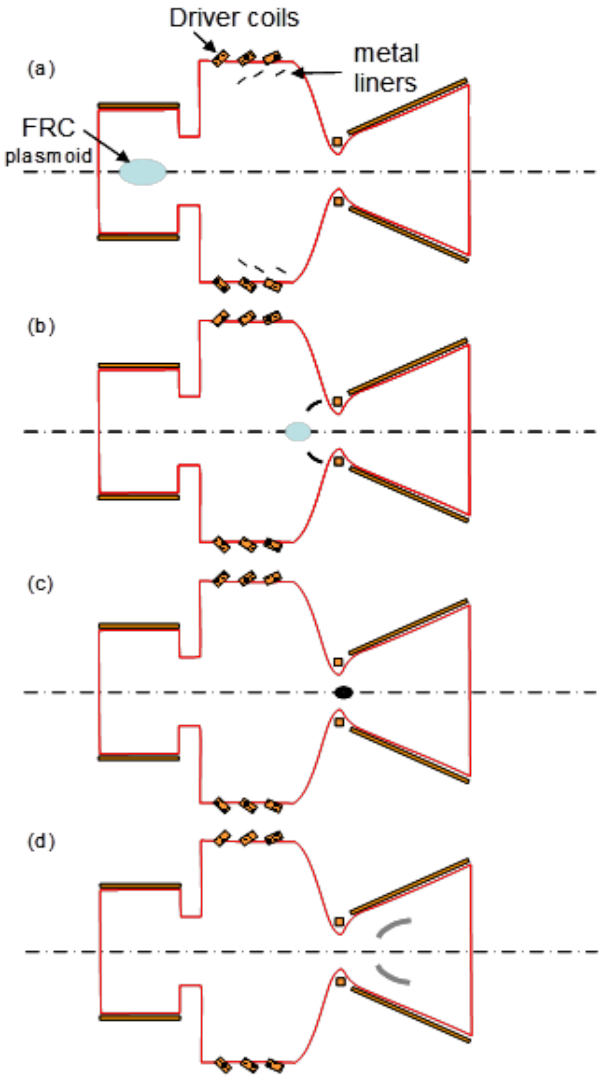

Fig. 2. Schematic of the IDLC for propulsion. (a) Thin hoops of lithium metal are driven at the proper angle and speed for convergence onto target plasmoid at thruster throat. (b) Target FRC is confined by axial magnetic field from shell driver coils as it translates through chamber eventually stagnating at the thruster throat. (c) Converging shell segments form fusion blanket compressing target FRC plasmoid to fusion conditions. (d) Vaporized and ionized by fusion neutrons and alphas, the plasma blanket expands against the divergent magnetic field resulting in a directed flow of the metal plasma out of the magnetic nozzle (magnetic fields not shown for clarity).

Finally, a straightforward way to convert the fusion energy into heat or propulsive energy must be realized. It is in this regard that the approach outlined here is uniquely capable. It starts by employing an inductively driven thin metal liner first to compress the magnetized plasma. As the radial and axial compression proceeds, this liner coalesces to form a thick ($r > 5$ cm) shell that acts as a fusion blanket that absorbs virtually all the fusion energy as well as the radiated plasma energy during the brief fusion burn time. This superheated blanket material is subsequently vaporized and ionized and now expands outwardly into the remnant magnetic flux used to drive the liners inward. It is possible to extract electrical energy directly from the back emf experienced by the magnetic driver field coil circuit as the reactor chamber flux is now convected and compressed by the expanding liner plasma. For the large compression/expansion ratios achievable the efficiency of this conversion can be as high as 90%.[14] For propulsion this expansion would occur inside the divergent magnetic field of the nozzle that converts this blanket plasma energy into propulsive thrust. A schematic depiction of how this would be accomplished can be found in Fig. 2.

III. PHYSICS OF THE IDLC

The analysis of the liner implosion was carried out for both a subscale validation experiment that could be performed with existing equipment at MSNW and the Plasma Dynamics Laboratory at the University of Washington, as well as a full-scale reactor prototype. For the purposes of the analysis given here, a very conservative liner kinetic energy, E_L = 560 kJ was assumed from the existing 1.4 MJ capacitor bank based on modeling and other inductive liner compression experiments.[4,13] The dynamics of the liner implosion are governed by the equation:

$$M_L \frac{d^2 r}{dt^2} = \left(\frac{B_{in}^2}{2\mu_0} - \frac{B_{ext}^2}{2\mu_0} \right) 2\pi r w \qquad (1)$$

where M_L is the liner mass, and w the liner width. During the liner acceleration very little flux leaks through the liner ($B_{in} << B_{ext}$). On energizing the driver coil, due to the small gap and the inertia of a solid metal liner, the magnetic field rapidly increases and is then maintained at a roughly constant amplitude ($B_{ext} \sim$ const.) during the inward motion of the

liner as the increasing flux from the driver circuit into the gap between the coil and liner is countered by the increasing gap cross-sectional area. This liner/magnetic behavior was confirmed by 3D modeling with the Maxwell® 3D electromagnetic code. With this approximation Eq. (1) is readily integrated. Given the liner mass $M_L = 2\pi r_L \cdot w \cdot \delta \cdot \rho_L$, where δ is the liner thickness and ρ_L the liner density, the liner velocity is:

$$v_L = \left(\frac{r(t)}{2\mu_0 r_L \delta \rho_L} \right) B_{ext}^2 t \quad = 125 \frac{\tau}{\delta} B_{ext}^2 , \qquad (2)$$

where τ is the period of acceleration at constant B_{ext}. An aluminum liner was assumed in evaluating the right hand side of Eq. (2). B_{ext}, is determined by the stored capacitor energy minus liner energy which is (1.4-0.56) MJ ~ 0.8 MJ for the PDL fast energy delivery system. Equating this to the magnetic energy stored in the annular of gap of the liners yields B_{ext} = 9 T when the liner has moved inward by 15% of the initial coil (liner) radius of 0.4 m. While the liner continues to be accelerated, the rate drops dramatically as the area between the coil and liner grows while the capacitor bank energy has been fully transferred to the coil. For the liner to have moved inward 6 cm in 40 μsec under a constant magnetic force implies a terminal velocity of v_L = 3 km/s, consistent with that predicted by the above equation for a 0.2 mm aluminum liner.

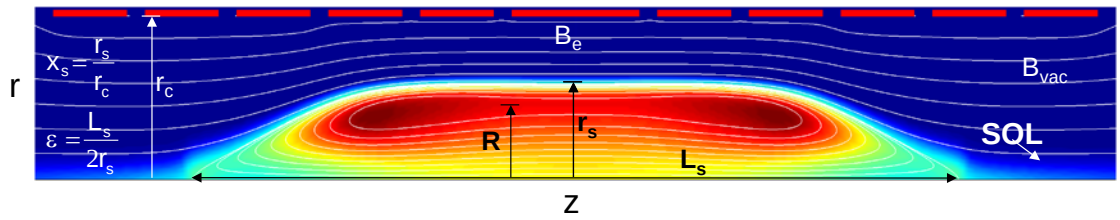

Fig. 3. Elongated Field Reversed Configuration (FRC) Equilibrium Magnetic Field lines and Pressure Contours

The key process of the dynamical behavior of the convergent aluminum foil liners was also analyzed with the ANSYS Multiphysics® code. Here the non-linear behavior of the aluminum liners was modeled based on the magnetic pressure profile in time and space similar to that predicted by Eq. (1) and Maxwell®. The result from a calculation with the physical setup similar to the subscale validation experiment is illustrated in Fig. 1.

As mentioned, the FRC has been selected as the target plasmoid. A schematic of FRC is shown in Fig. 3. The liner moves in radially compressing the FRC until it stagnates due to the rising pressure from the trapped magnetic field (and FRC plasma). The energy within

the FRC separatrix at peak compression is dominated by plasma energy that must be in radial pressure balance with the edge axial magnetic field B_0, so that one can write:

$$E_L = \frac{1}{2} M_L \, v_L^2 = 3 n_0 \, k T_0 \cdot \frac{4}{3} \pi \, r_0^3 \varepsilon = \frac{B_0^2}{\mu_0} \pi \, r_0^3 \varepsilon \qquad (3)$$

where the zero subscript indicates values at peak compression. The last expression in Eq. (3) reflects the reasonable assumption that $r_s \sim r_0$ and magnetic pressure balance ($2n_0kT_0 = B_0^2/2\mu_0$). One has then for the fusion energy produced in the FRC during the shell's dwell time τ_D at peak compression:

$$E_{fus} \cong \; 1.2\times10^{-12} \, n_0^2 \, \langle \sigma v \rangle \, \frac{4}{3} \pi \, r_0^3 \, \varepsilon \, \tau_D \;\; = \;\; 1.1\times10^{-42} \, n_0^2 \, T_0^2 \, \frac{r_0^4}{v_L} \varepsilon \qquad (4)$$

where n_0 and T_0 are the peak density and temperature, and where the liner shell dwell time at peak compression, τ_D, $\sim 2r_0/v_L$. The dwell time can actually be much longer for a thick liner, but the more conservative dwell time is assumed here. Liner compressive effects are also ignored in this zero order analysis. The usual approximation for the D-T fusion cross section in this temperature range: $\langle \sigma v \rangle \cong 1.1\text{x}10^{-31} \; T^2(\text{eV})$ was also assumed. Pressure balance, together with expressions (3) and (4) yields for the fusion gain:

$$G = \frac{E_{fus}}{E_L} \;\; = \;\; 1.73\times10^{-3} \sqrt{\frac{M_L}{l_0}} \, B_0 \;\; = \;\; 4.3\times10^{-8} \sqrt{M_L} \; E_L^{11/8} \qquad (5)$$

where l_0 ($= 2r_0 \cdot \varepsilon$) is the length of the FRC at peak compression. The last expression is obtained from the adiabatic scaling laws for the FRC:[15]

$$E_L \sim B_0^2 \, r_0^2 \, l_0 \sim B_0^{4/5} \qquad l_0 \sim r_0^{2/5} \sim B_0^{-1/5} \qquad (6)$$

in order to express G in terms of the liner kinetic energy and mass, E_L and M_L only.

Starting with typical FRC parameters one obtains the final FRC parameters assuming both an adiabatic radial and axial compression from the 3D convergence of the liners. The ends of the merged liners are observed to do this naturally in the ANSYS® calculations (see Fig.

1), as the end liners have a significant axial velocity component and are unimpeded by the FRC presence as it contracts axially inward. The unique behavior of the FRC equilibrium to axial liner compression is quite valuable in this context as it provides for magnetic insulation of the FRC boundary regardless of the increase in the ratio of plasma to magnetic energy that comes with the increased axial compression. The proper plasma parameters for the initial FRC are found by extrapolation back from the desired final state. The compression that is applied by the liners is adiabatic with regard to FRC as the liner motion is far less than the plasma sound speed. The key adiabatic relations for the FRC are stated in Fig. 4.

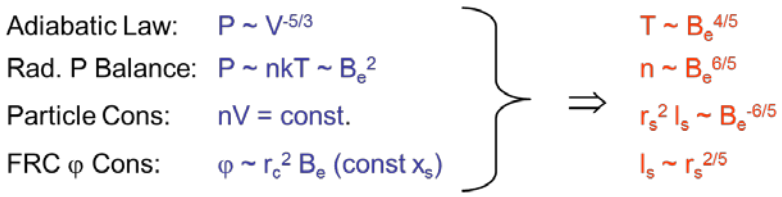

Fig. 4 FRC adiabatic scaling laws used to obtain initial FRC conditions from the desired conditions at full compression.

Injecting the FRC into the liners is delayed to until the liners have been fully accelerated and have moved inward away from the driver coils. For the validation experiment this would be accomplished by injecting two FRCs and merging them inside the liner as this permits an axially stationary liner compression which considerably eases the diagnostic evaluation of the compression process as the target remains fixed. Adding a translating component to the liner motion would be something to be addressed for the space propulsion application after success with the validation experiment.

IV. IDLC VALIDATION

As mentioned the scale of the validation experiments is based on the generation of an FRC similar to that produced in the LSX FRC experiments.[5] Using the FRC adiabatic scaling laws listed in Fig. 4, and assuming E_L = 560 kJ, the convergence of a set of three aluminum liner set with an initial total mass of 0.18 kg would produce a peak edge magnetic field of 410 T (see Fig. 5), with a compressed FRC length of 35 mm. From Eq. (5) a fusion gain G = 1.5 would result. If realized, this would be a remarkable achievement for such a modest experiment and would act as a testament to the cost and efficiency advantages of this approach to fusion.

The total gain desired from the IDLC is determined by the energy requirements to vaporize, ionize and energize the metal liner propellant to achieve a suitably robust plasma expansion

or directed momentum for the space application. It is useful then to rewrite Eq. (5) in terms of the fusion energy produced per unit liner mass:

$$\frac{E_{fus}}{M_L} = G\left(\frac{E_L}{M_L}\right) = 4.3\times10^{-8}\, M_L^{15/8}\, v_L^{4.75} \tag{7}$$

where Eq. (3) was used to put the expression in terms of the explicit liner variables. It can be seen that increasing either the liner mass, or velocity will increase the energy input into each liner particle.

Parameter	Merged FRC ($t = \tau_{1/4}$)	Radial FRC Compression	Axial FRC Compression
v_L (km/s)	2.5	~ 0	0
r_L (cm)	22.5	0.9	0.9
r_s (cm)	20	0.8	0.88
l_s (cm)	80	22	3.5
B_{ext} (T)	0.16	100	410
T_e+T_i (keV)	0.06	5	15
n (m^{-3})	1.1×10^{21}	2.5×10^{24}	1.4×10^{25}
E_p (kJ)	2.2	180	560
E (Pa)	1.5×10^{4}	6×10^{9}	10^{11}
τ_N (μs)	600	175	270

Fig. 5. Anticipated FRC parameters from the validation experiment from merging, followed by a purely radial, and a purely axial compression. In the actual experiment the FRC radial and axial compressions would occur simultaneously.

IV.A. Evaluation criteria for the metal liner

There is however a velocity limit for a given liner thickness. This set by a material's properties (electrical conductivity, melting point, and heat capacity) in order to avoid vaporization due to the inductive heating that the liner experiences during magnetic acceleration of the liner. As was first pointed out by Cnare in his landmark foil compression experiments, the liner's minimum thickness (mass) for a given liner velocity can be characterized by a parameter g_M defined by the "current integral":

$$\int_0^{t_m} I^2 dt = g_M A^2 \qquad (8)$$

where I is the current flowing through the material cross-sectional area, A = w×δ, and where w is the hoop width and δ the hoop thickness. The driving force is simply the magnetic pressure ($B^2/2\mu_0$) applied over the surface area of the metal shell facing the coil when in close proximity to the driving coil. The current can be related to the force through Ampere's law which can be reasonably approximated as $B = \mu_0 I/w$. Normalizing to the action constant, g_{Al} for the vaporization of aluminum from an initial 300 °K, one finds for the maximum velocity for a given shell thickness δ:

$$v_{\max} = 6.8x10^{10} \frac{g_M}{g_{Al}} \frac{\delta}{\rho_M}, \qquad (9)$$

where ρ_M is the shell material density. This should not be a significant issue during field compression due to the formation of a thick blanket at convergence. The initial thickness will typically be much greater than needed for the characteristic velocities (2-4 km/s) anticipated.

There are potentially several metals that could be employed. Not surprisingly, aluminum is a strong contender due to its low density and high conductivity, but lithium is not far behind. Possessing a low yield strength, a lithium liner would be especially advantageous in that the initial thin shell could be readily extruded for positioning under the driver coils between pulses. For a given liner energy, its low mass density allows for thicker initial liner as well as a larger final shell radius. The latter is important for slowing down the fusion neutrons and extracting the maximum energy from the fusion products. Lithium also has several advantages as a plasma propellant. Recall that the ultimate fate of the shell is vaporization and ionization after intense fusion, Ohmic and radiative heating. For the space propulsion application lithium is to be favored for its low ionization energy thereby minimizing the frozen flow losses. Due to its low atomic mass it will also attain the highest exhaust velocity for a given fusion energy yield. For these reasons, lithium is the material of choice for the IDLC. From Eq. (9) one finds for lithium: v_{max} (km/s) = 16·δ(mm). The anticipated lithium liner thickness is several mm so there is no real issue here as high gain can be accomplished with liner velocities of 3-4 km/s. For the validation experiment aluminum is the clear choice due to its wide availability, low cost, and ease in handling.

IV.B. Validation Experiment

The basic approach will be to test liner convergence with aluminum liners using the G-10 vacuum chamber and driver coil pair used for the Foil Liner Compression experimental

testing at MSNW, but powered by the full energy storage and delivery system at the UW Plasma Dynamics Laboratory. The principle diagnostics to determine liner position as a function of time will be internal magnetic probes on axis, and axial arrays of external flux and B loops. End-on imaging of the liners will be obtained with a backlit fast framing camera. As in other liner experiments, both at MSNW and elsewhere[12,13] these images yield detailed information regarding liner uniformity during convergence. The liners will be constructed out of 6 cm wide, 0.2 mm thick aluminum strip and joined using an ultrasonic welding technique that maintains the structural, thermal and resistive properties of the material.

Detailed 2D, resistive Magneto-Hydrodynamic (MHD) calculations have been carried out to study the FRC formation and merging in this geometry, first with three and then two converging liner bands. It appears that for the *in situ* case (no overall translation of the liners as in Fig. 6), that two should be sufficient to assure proper axial and radial compression of the FRC. Internal rings can be employed if necessary. The result from a 2D MHD calculation of FRC merging with three rings is shown in Fig. 7. The primary diagnostic of plasma compression and heating is the neutron count from the D-D fusion reaction. The yield is a sensitive measure of ion temperature. The signal will be analyzed using MCNP codes used in previous FRC experiments.[16] A soft x-ray camera was used for plasma imaging and electron temperature measurements. Plasma density was obtained from a cross-chamber HeNe laser-based interferometer.

The principle task of the project was to design and assemble the foil liner FRC formation chamber, the full compression test structure and chamber including the compression bank. The second task was to test foils in the test facility constructed in year one and characterize the performance obtained from liner compression. These experimental measurements were then compared with analytical predictions, and numerical code results. The liner testing was completed and compared with both the analytical results as well as the code work performed with the 3D structural dynamics package of ANSYS Multiphysics. This code is capable of modeling the dynamic behavior of materials well into the non-linear regime (e.g. a bullet hit plate glass). The liner dynamic behavior was found to be remarkably close to that predicted by the 3D structural dynamics results. Incorporating a code that can also include the magnetics and plasma physics has also made significant progress at the UW. The remaining test bed construction and assembly task was completed by the end of the second year. The FRC formation and merging experiments were carried out as planned. The liner compression of the FRC to megagauss fields was not performed due to not obtaining a sufficently long lived FRC during the final year of the grant.

It was decided that it was essential to have to have a segmented foil with each foil of the multi-foil array to be imploded onto the FRC as an independently controllable event. This added considerably to the design and fabrication costs, The coil independence is essential to obtain the full three dimensional compression of the FRC, which is a unique capability of inductive method for liner compression. It was also required in order to operate the compression section as a two turn coil there by necessitating a bit more effort in control

hardware as well as a much more complex machining effort on the magnets. With full control of both the timing and force of foil acceleration much greater compression can be obtained. With successful results from these experiments, a sub-megajoule system could be assembled from existing hardware to create a breakeven foil liner compression experiment. The advantages of the inductively driven, 3D foil liner implosion for obtaining megabar pressures and fusion gain conditions is discussed in a separate paper to be submitted.

The FRC formation chambers have been constructed (see Fig. 6), and the high field compression coils were machined and encapsulated. There have been issues here. Driving the coils as a set of nine two-turn coil pairs was deemed necessary to increase the bank coupling to the foil as the presence of the foil acts to effectively short out the coil during drive. The substantial increase in coil current demand during liner drive is also better handled with the two turn approach. In order for there to be no substantial field error near

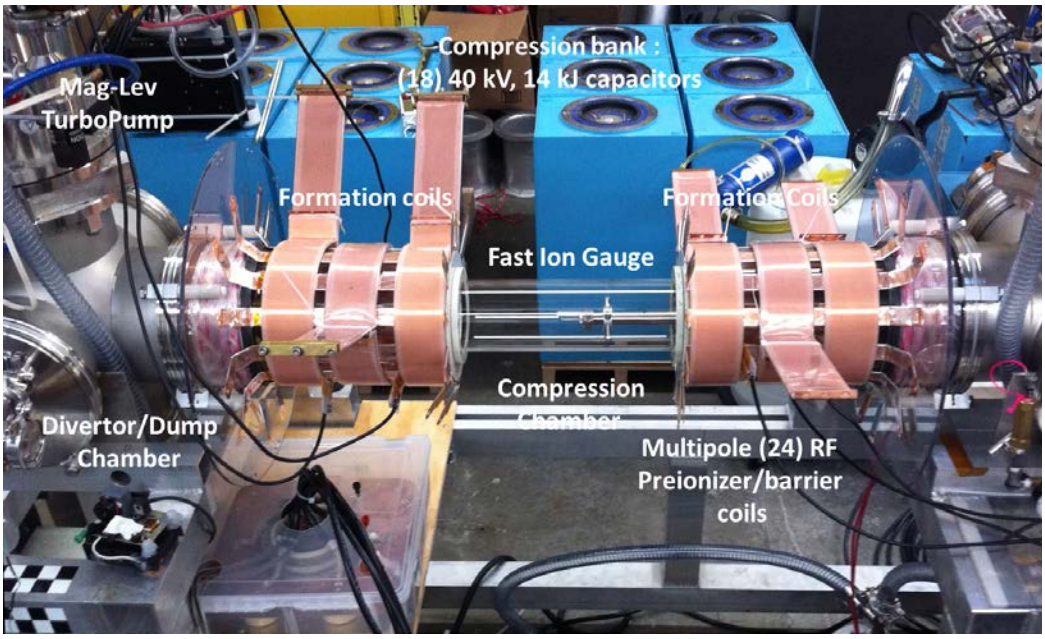

Figure 6. FLC experimental test bed prior to installation of cables and compression magnets. A duodecapole is rung at high frequency (4 MHz) to initiate gas breakdown prior to the standard ringing theta pinch preionization at each end of the FRC compression chamber. Axial (Fast ion gauge was used to measure gas arrival time to minimize neutral gas in compression chamber.)

the coil, the coil form was machined in a manner such that the current has only an azimuthal flow near the coil inner radius. A methodology for machining the coil has proven successful, and after several tries, a methodology for encapsulation was worked out, and the compression bank thoroughly tested on the foil liner test facility to be discussed in the next section.

Operating at only half power, 5 gram Aluminum liners have been accelerated to 1,800 m/s. This represents a directed energy of 8.1 kJ of the 21 kJ originally stored in the capacitors at initiation for an energy coupling efficiency of 38%. This efficiency is more than sufficient and will likely be increased with the use of flux concentrators. This is a new concept that will be developed in the follow on program with the supplemental funding. The initial driver coil was constructed as a three turn coil and was made from stainless steel wire to minimize pulse duration and therefore the impulse force on the coil. Other materials have been tested including brass and low carbon steel. The latter combines the best combination of high tensile strength and the appropriate resistivity to provide sufficient

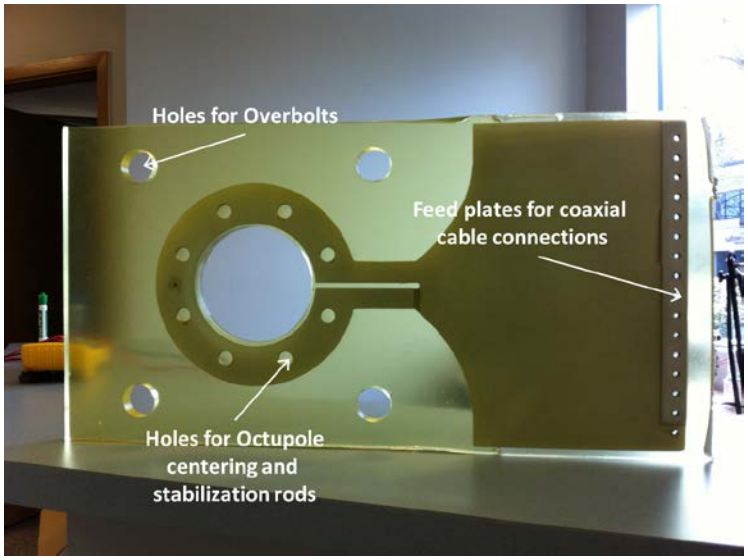

Figure 7. Prototype coil for FLC foil compression section

current on the short timescale of liner acceleration (~ 10 μsec), yet damp away quickly enough to minimize the impulse to the coil structure.

These coils were useful for the initial tests, but none of these coils were capable of tolerating the thousands of pulses that would be desired for long term experimentation. It was decided that a more robust coil was needed that could be pulsed to over 20 T indefinitely. The appropriate aluminum material was machined and encapsulated for high voltage (60 kV minimum). A picture of the prototype coil is shown in Fig. 7.

It worked flawlessly without measurable dimensional change for over one thousand pulses, and was deemed suitable for the 18 coil array for the foil compression bank. Two of the prototype coils were used in series on the foil test facility. This facility will continue to operate while the foil liner test bed is finished as well as during operation as different foil joining and manufacturing techniques are developed for future experiments. A picture of the final assembly of the FLC experiment is shown in Fig. 8.

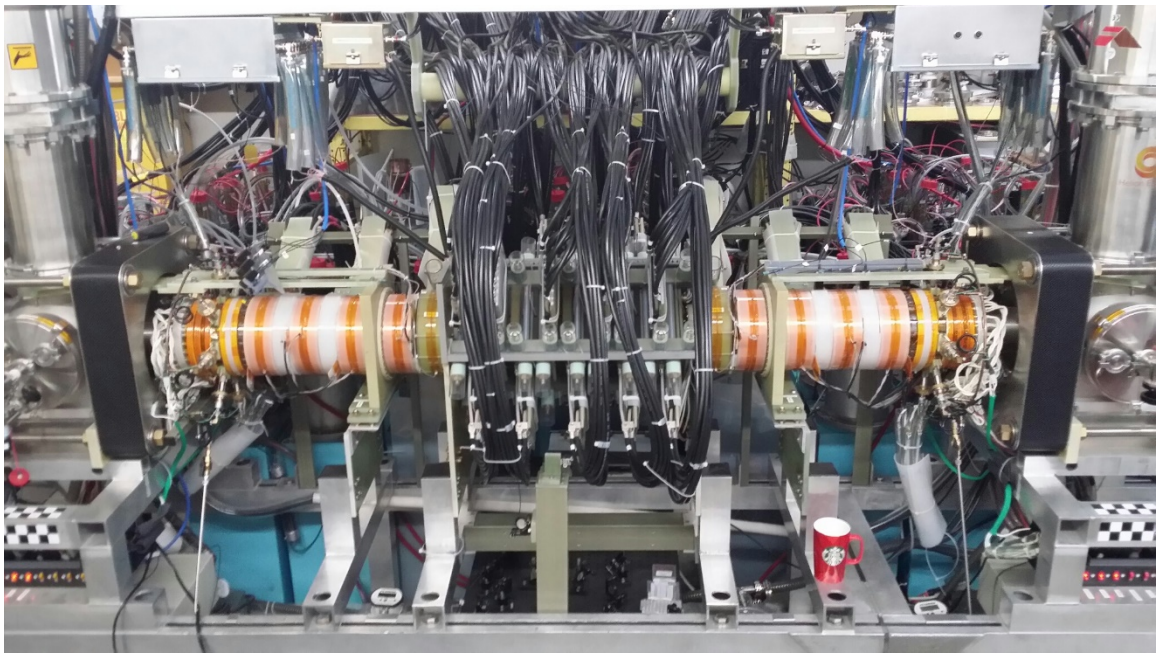

Figure 8. The final FLC experimental test bed employed to generate the target FRC through merging of two FRC. Cables feed the 20 high field coils used for flux and liner compression of the FRC.

Coil and Liner Design

The major task of the second year was to design a coil that could operate at a high energy transfer rate and deliver the requisite energy to the foil liner. This was completed and is pictured below in Fig. 9. The polyethylene tube was employed until a better understanding of the debris field was obtained. Surprisingly, even when the foil is completely disassembled and even partially melted, very little material is returned to the tube wall. There is however a powerful jet of liner material that imbedded aluminum fragments on axis at each end of the test chamber. This is surrounded by a larger cone of powdered material loosely bound to the surfaces. It appears that there is only minor damage to the tube walls that simple cleaning will restore, however there needed to be sacrificial discs placed at each end in the dump chambers to catch the high energy jets. In the test chamber this was typically a thin disk of polycarbonate so that end fast framing pictures of the liner dynamics could be obtained. A similar set-up would need to be used on the testbed experiments.

The desire was to have the foil achieve an inward velocity of 2 km/s (2 mm/μsec). At this speed the compression of a 4 cm radius FRC could be accomplished in 20 μsec. The plan is to start with a much larger formation chamber (r_c = 10 cm) and produce an FRC with a much longer lifetime (~ 100 μsec). While this may seem to be overkill, it must be remembered that the FRC lifetime is a strong function of r ($\tau \sim r^{2.1}$). While this is compensated somewhat by the FRC density scaling ($\tau \sim n^{0.6} \sim r^{(-2.4)0.6}$), the overall FRC

lifetime will decrease as it is compressed ($\tau \sim r^{0.66}$). For a ten to one radial compression the FRC lifetime will decrease by a factor 5. Since the reduction occurs during the compression, there should be more than adequate FRC life even if the compression speed were somewhat slower.

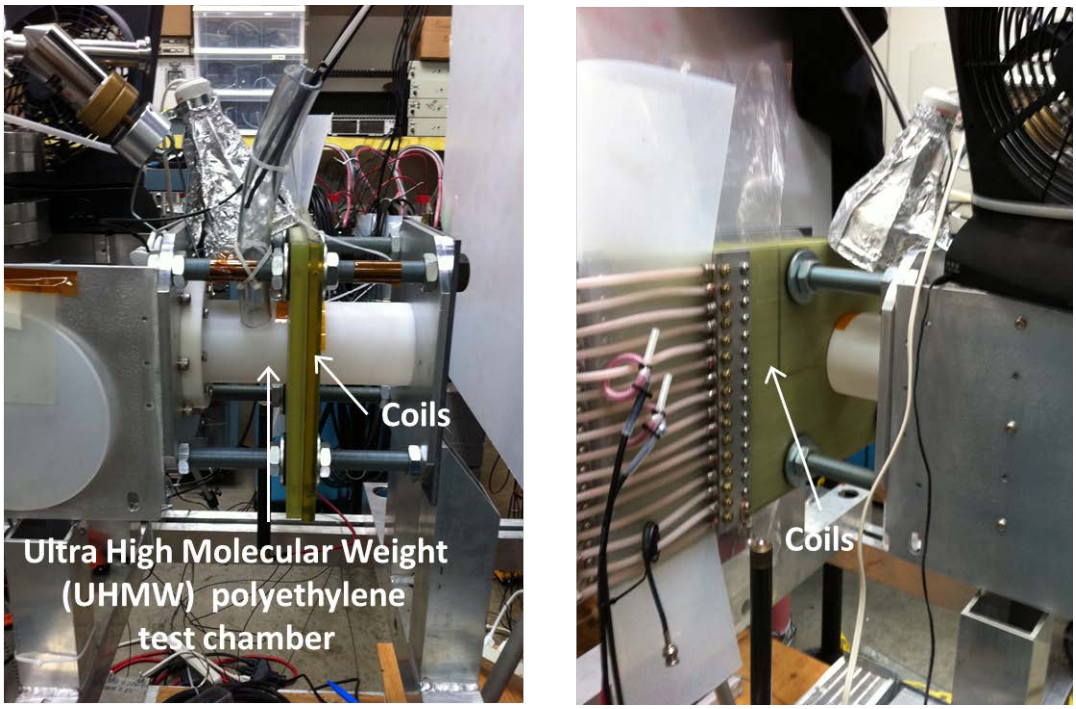

Figure 9. Foil compression test chamber.

The desire was to keep the energy involved in the liner implosion to a minimum so as to limit collateral damage. It was also decided to abandon the use of a solid dielectric breakdown for the switching. This technique had been used in the past as it provides for a very low stray inductance. Given the small size of the compression coils ($r_c \sim 5$ cm), this is important. Initial experimentation led to results that were far from optimal. The time spent in getting the dielectric to yield was large, and the jitter was essentially uncontrollable on the sub microsecond timescale desired. This was an important as the desire was to have the ability to modify the compression profile. This could be done by having various liner segments have different masses, speeds and most importantly, timings. The decision was made to employ the thyratron switches we use for the FRC formation to gain more control as well as eliminate the time that would be spent in regenerating the switches after discharge. It also provided for a means to crowbar the coil current thereby maintain the radial pressure on the liner and thus increasing the time for liner acceleration. A picture of the test bank, cables and switches is found in Figs. 9 and 10.

As was first pointed out by Cnare in his landmark foil compression experiments, a material's electrical and thermal properties determine the shell's minimum thickness (mass) for a given shell velocity (energy) when driven by the inductive technique in order

to avoid vaporization. The material properties relating to this resistive heating (electrical conductivity, melting point, heat capacity, etc.) can be characterized by a parameter g_M defined by the "current integral":

$$\int_0^{t_m} I^2 dt = g_M A^2 \tag{10}$$

where I is the current flowing through the material cross-sectional area, A = w×δ, where w is the hoop width and δ is the hoop thickness. The driving force is simply the magnetic pressure ($B^2/2\mu_0$) applied over the surface area of the metal shell facing the coil when in close proximity to the driving coil. The current can be related to the force through Ampere's law which can be reasonably approximated as $B = \mu_0 I/w$. Normalizing to the action constant, g_{Al} for the vaporization of aluminum from an initial 300 °K, one finds for the maximum velocity for a given shell thickness δ:

Figure 10. Prototype pulse power system employed on the liner test facility.

$$v_m = 6.8x10^{10} \frac{g_M}{g_{Al}} \frac{\delta}{\rho_M}, \tag{11}$$

where ρ_M is the shell material density. This should not be a significant issue during field compression due to the formation of a thick shell at convergence. The initial thickness will typically be much greater than needed for the characteristic velocities (2-3 km/s) anticipated. The maximum velocity for various materials is given in Fig. 11.

Element	Current Intgrl.	Ratio to Al	v_{max}/δ (m/s)	Ratio to Al
Ag	1.53E+17	1.51	9.19E+06	0.39
Al	1.01E+17	1.00	2.37E+07	1.00
Al (6061)	1.07E+17	1.05	2.49E+07	1.05
Au	1.39E+17	1.37	4.53E+06	0.19
Be	9.24E+16	0.91	3.15E+07	1.33
Cu	**2.33E+17**	**2.30**	1.64E+07	0.69
Li	1.36E+16	0.13	1.61E+07	0.68
Na	1.19E+16	0.12	7.70E+06	0.33
Pb	5.79E+15	0.06	3.21E+05	0.01
Mg	2.20E+16	0.22	7.95E+06	0.34

Figure 11. Candidate metallic liner materials

It is easy to see that aluminum is the best liner material (actually Beryllium is marginally better but nearly impossible to use). For a given velocity the minimum liner thickness is determined by Eq. (11). For v_m = 2 km/sec one has δ_L = 43 microns ~ 1.7 mil in American units. It was found experimentally that a much thicker liner is required as the heating of the liner also rapidly increases the resistivity of the conductor. We observed liner vaporization for liners with a thickness less than 5 mil. Given a correction factor of 3 based on experiment then one has:

$$E_L = \rho_{Al}\, 2\pi r_L\, \delta\, l_L\, v_L^2 \qquad (12)$$

With ρ_{Al} = 2,700 kg/m^3, δ = 0.15 mm (6 mil), and v_L = 2 km/sec, one has

$$E_L = 10.2\ r_L \cdot l_L \text{ (MJ)}. \qquad (13)$$

Where r_L is the liner radius and l_L is the liner length. Clearly one wishes to minimize both of these. The minimum radius for the initial liner is set by the need to inject a mWb scale FRC into the liner. It may be possible to pre-compress the FRC to smaller radius than 4 cm, but it was decided that would risk even more rapid decay of the FRC. It could also engender the rotational instability prior to insertion in the metal liner making translation difficult. It is expected that the conducting liner will help prevent wall interactions with a rotating FRC once inserted. The minimum radius was chosen to be 5 cm. The total length

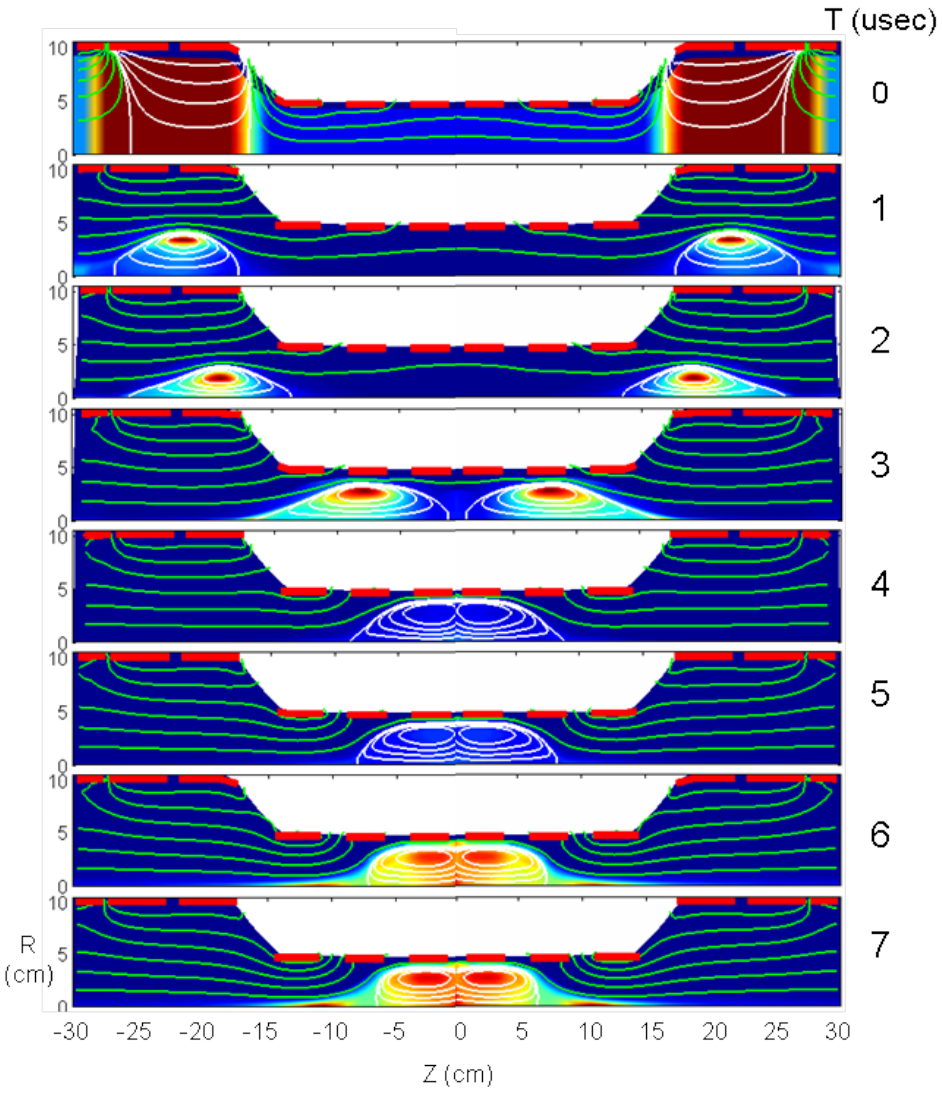

Figure 12. 2D MHD calculation of FRC formation and merging for the foil liner experiment. It was assumed that the liner motion has been initiated earlier and that the liners (central four coils) are at a 4.5 cm radius. The liner motion is not part of the calculation as the coils are at fixed radius in the Moqui code. A new code is being developed at the UW to include liner motion and behavior.

of the liner is adjustable as it is comprised of several short segments to make for simpler operation from both switches and coils, as well as provide for 3D liner compression. A segmented liner also limits the impact of a prefire of one of the switches. From 2D MHD calculations with Moqui it was decided that a total of four liners, each 3 cm in length, covering an axial span of roughly 20 cm would be sufficient to compress the merged FRC from the two larger source section (see Fig. 12). The driver coils are the same length as the liner segments. As can be seen in Fig. 12 an additional driver coil at each end was used to

Figure 13. (top) 3 mil copper foil. (bottom) 6 mil aluminum foil

provide a strong mirror preventing FRC expansion or translation during the liner compression. These coils will be similar to the liner drivers so that a larger liner, or preferably a liner segment that can be driven both axially and radially inward can be employed.

The energy required to drive each foil liner section then can be determined from Eq. 13 with the result: E_L =15 kJ.

It is believed that the efficiency of the energy transfer from the capacitor to the liner can be as high as 50% with the proper magnetic waveform it will be assumed to a more conservative 35% in line with the efficiencies obtained with the foil tests. The stored energy

per foil segment thus needs to be ~ 44 kJ. For the minimum of four liner segments, this will require a total stored energy of 175 kJ. The compression bank has over 240 kJ of stored energy to assure that the desired liner energy is achieved even if the efficiency isn't as good as anticipated.

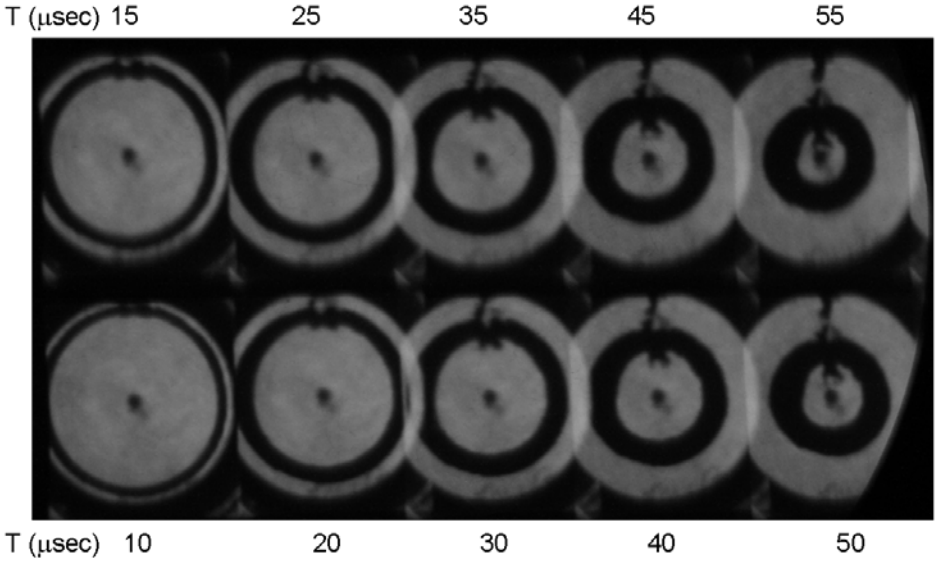

Figure 14. Sequence of framing pictures taken during liner compression at ¼ power. The Aluminum liner was a multi-turn 1 mil foil with a total thickness of 6 mils (3.5 g). Tape shadow can be seen on both the outside and inside of liner.

The foil liner tests were conducted with a liner radius of 4.3 cm and 5 cm, with lengths of 2 to 4 cm. A picture of the test coils, chamber is shown in Fig. 9. A picture of a copper and an aluminum test foils is shown in Fig. 13.

Two single turn coils were driven in series were constructed as shown in Fig. 7. A suitable urethane casting compound was found that has a dielectric strength of 1,200 V/mil as is quite strong much more tolerant of shock loading than epoxy encapsulants.

The foil itself was constructed in a unique way. It is difficult to machine a cylinder to uniform thickness when the wall dimensions are as small as only a few mils. A uniform and variable wall thickness was obtained by employing a thin 1 mil foil and circumscribing the inner wall radius of the chamber as many times as desired to obtain the proper thickness desired. The composite liner was then spot welded at 6 azimuthal locations to assure structural rigidity and current sharing among the layers. The skin depth is larger than the total liner thickness so that the entire liner should carry current. The bulk of the testing was done with a liner of 6 turns, in other words a 6 mil thick liner. The large cross sectional area between the turns allowed for current to travel azimuthally without increased resistance in passing from turn to turn. The only issue was the high temperatures of the liner causing the aluminum to melt at the welds. This tended to created a very bright image on the end-on framing pictures. At less compression power this did not occur. A picture

sequence for a ¼ power discharge is found in Fig. 14. Better liner symmetry is obtained with higher power. Even without the end-on images, the liner behavior can be obtained from the internal B_i, external B_e, and flux F loops. They are related by the following equation:

$$F(t) = B_e(t)\pi r_{loop}^2 + B_i(t)\pi r_L^2(t)\,. \tag{14}$$

The internal probe consists of a four turn winding on a 1.5 mm diameter alumina tube with the leads returned through the bore. The flux loop is a single turn winding positioned around the chamber wall under the driver coils. The external field loop is a small loop

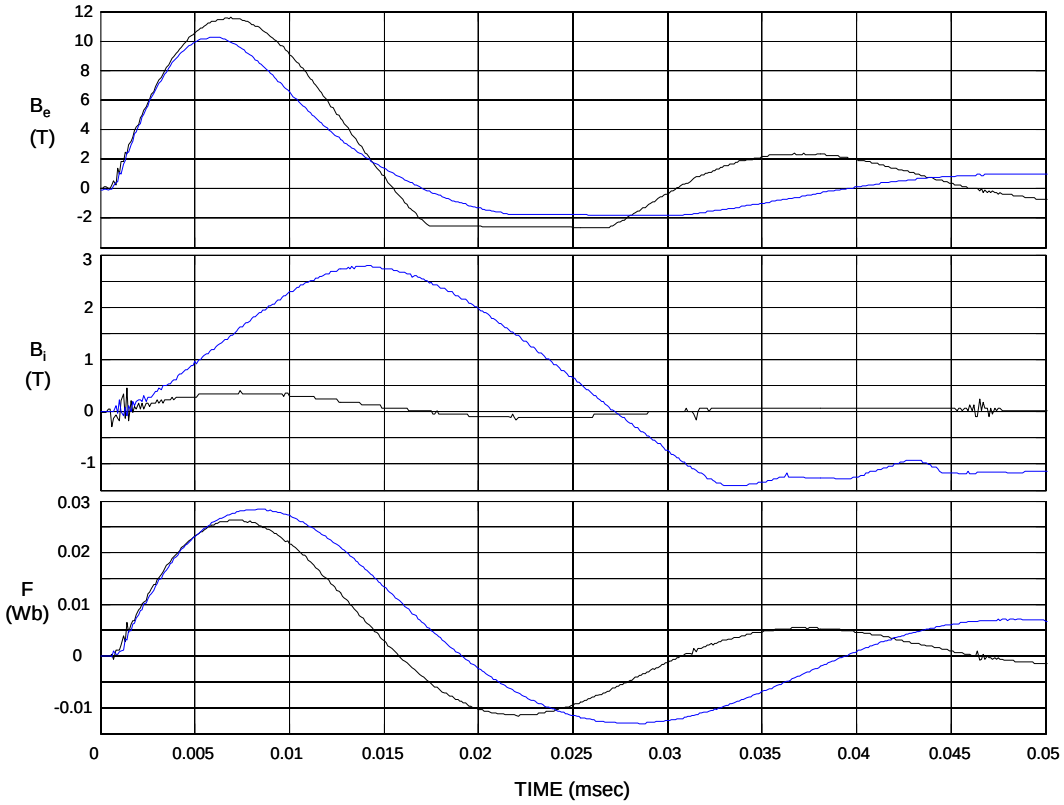

Figure 15. Time histories of the external axial magnetic field, B_e, on axis internal axial magnetic field, B_i, and flux inside the liner driver coil, F. Blue traces are from discharge with a 6 mil Aluminum liner implosion and black traces are from a discharge with a fixed Aluminum cylinder of the same initial radius as the foil.

embedded in an azimuthal groove placed in the polycarbonate wall, and is thereby positioned in the gap between the driver coil and foil liner. Plots of the three magnetic

measurements during a foil liner implosion are shown in Fig. 15. Also included in the plots are the measurements with a thick walled (1/4”) aluminum cylinder substituted in place of the foil so that the probe array can be checked against a fixed and known liner radius. The departure of the blue (foil liner) trace from the black (fixed cylinder) trace indicates the time when the liner begins to move inward. It can be seen from the internal B trace that the field that leaks through the liner is then compressed by the liner later in time as desired.

Since the B loop radius is known, the liner radius r_L can be solved for at all times. A plot for a half power discharge is shown in Fig. 16. From this figure the terminal velocity of the liner can be obtained. The glitches in the plot are due to the indeterminacy of the radius as

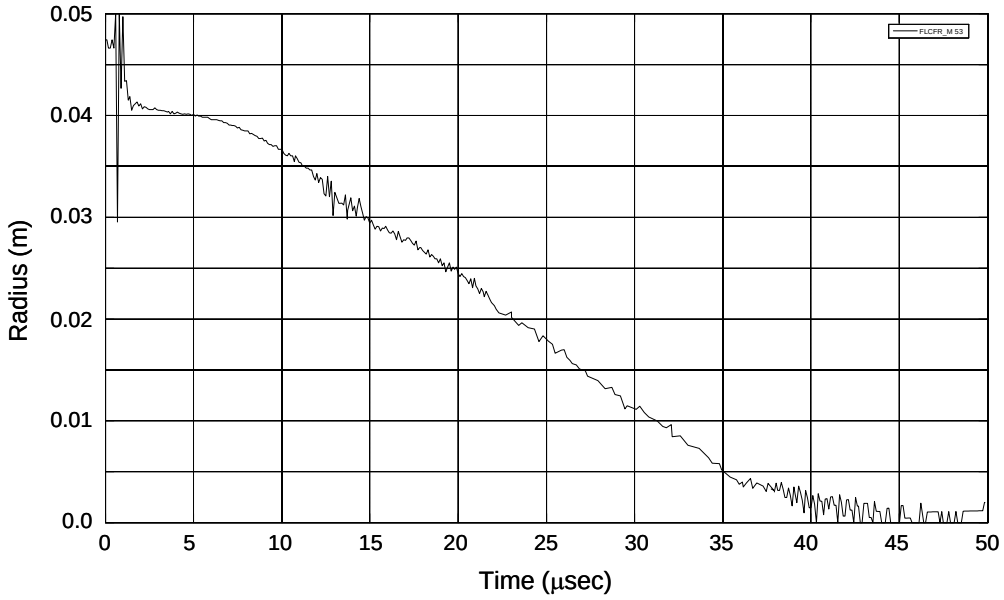

Figure 16. Foil liner radius determine by internal B and external B and flux measurements

the external field passing through zero since no crowbar was used on this discharge. The crowbar was unnecessary as the stainless steel coil resistance decays the field so rapidly that there was no real reason to use it. It is clear from the trace in Fig. 16 that the active acceleration of the liner has essentially ended by 10 microseconds. The maintenance of the field for the first 10 microseconds and later is important to deliver the largest force for the longest time. As can be seen the flux will leak out of the liner if the compression process is too long and the field external to the liner is allowed to decrease and even reverse.

Foil Liner Numerical Calculations

The original plan was to modify the Mach2 code that has been used previously for Z-pinch (B_θ) compression of metal liners. It was discovered that the Mach2 code was incapable of operation with inductively driven (B_z) liners. At that point it was decided to pursue a new 3D code based on the COMSOL CFD code for incorporation of the liner with a simple cylindrical liner, and a structural dynamics code – ANSYS Multiphysics® for the liner dynamics. This is also a 3D finite element code that can incorporate electromagnetics as well. The results from the ANSYS calculations conducted at MSNW will be covered first with the approach taken as the UW to follow.

It was decided to initially explore the liner behavior without the final magnetic compression as the physics of liner acceleration and the post implosion behavior is only marginally influenced by the bleed-through flux. While this flux is important for magnetic isolation of the FRC, it has no significant effect on the liner implosion for all but the last microsecond. The ANSYS code was set up with the appropriate stress-strain and yield strength for the Aluminum (6061 and 1000 series) that we employed in the tests. The magnetic impulse was modeled by a pressure profile matched to that from the experimental coil magnetic pressure both spatially and temporally. The grid mesh for the calculations is shown in Fig. 17 and the results from a sample calculation are shown in Fig. 18.

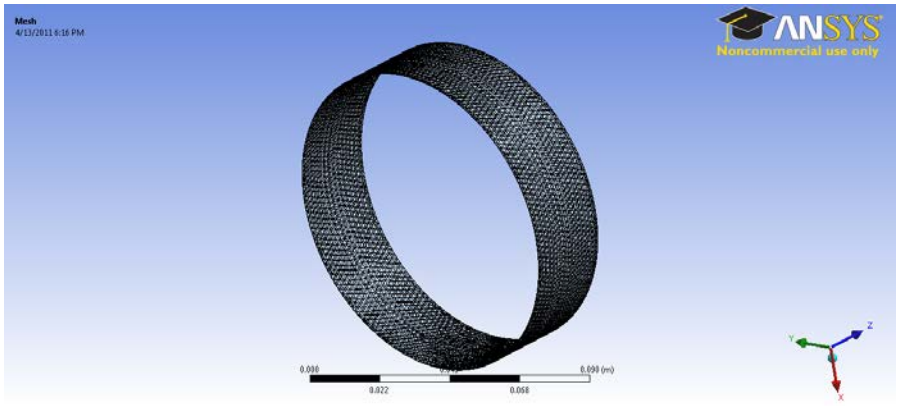

Figure 17. Mesh used for structural dynamics of liner compression.

The high grid resolution was required for convergence as well as capturing the behavior of an object whose thickness is several orders of magnitude smaller than the other dimension. It is rather remarkable that the code can follow not only the dynamics of the thin liner, but resolve the fine structure behavior such as the intricate buckling as can be seen in Fig. 18. For this case the magnetic pressure was less than the yield strength of the Aluminum (40 MPa vs 150 Mpa). With excellent implosion symmetry a uniform, high order buckling is observed in both the numerical calculations and the experiments. A testament to the

accuracy of the calculations was the predicted velocity of the liner as well as the degree of buckling.

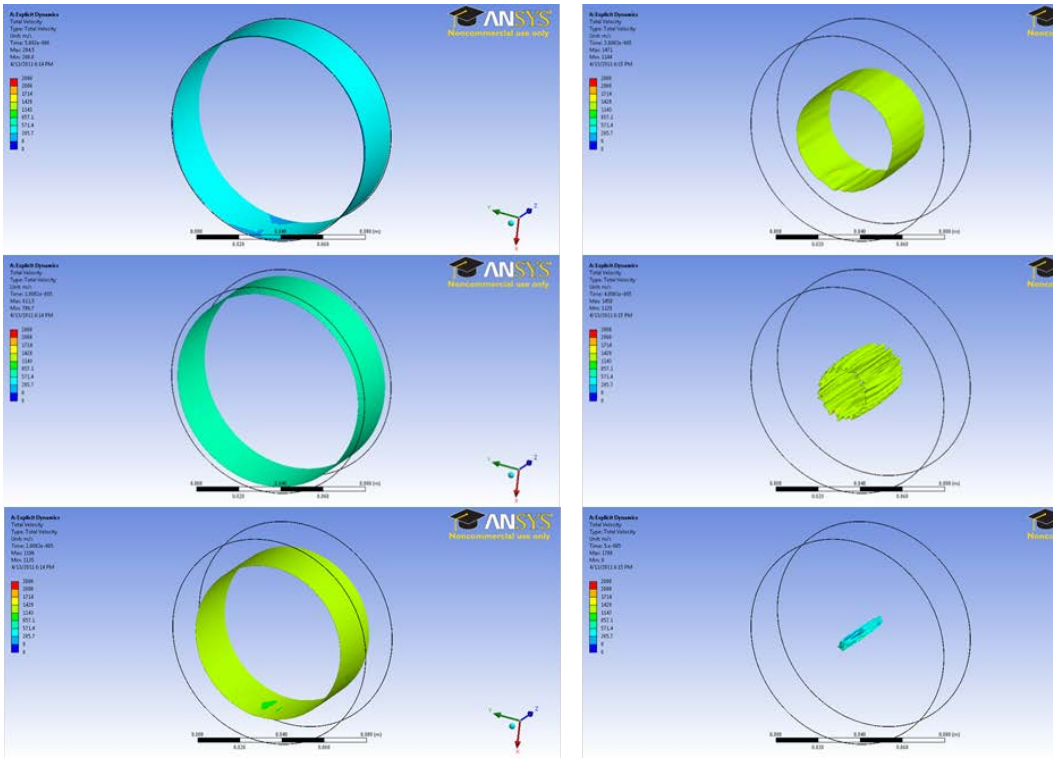

Figure 18. Compression of a 6 mil Aluminum liner with a 10 T peak magnetic field. Time steps are 5, 10, 20, 30, 40, 50 μsec. Color indicates radial velocity. Red ⇔ 2.0 km/s.

When the field was raised to match the yield strength of the Aluminum, the liner was observed to disintegrate on implosion. This same phenomena was also observed in the code. A series of snapshots of the liner under these conditions is shown in Fig. 19.

At even higher fields, well beyond the yield strength, it is observed that the buckling depth becomes even smaller and appears relatively late in the implosion. The speed for the liner in Fig. 18 was ~ 2 km/s (2 mm/μsec) which is the target speed. There is sufficient bank energy and voltage to produce faster and more energetic implosions. This would only be done if the FRC lifetime is less than anticipated.

The next improvement to the ANSYS calculations was to incorporate a pitched coil launch capable of adding an axial velocity component as this would provide for the most efficient use of the bank energy in a truly 3D compression of the FRC. The initial tests indicate that such a liner motion is quite doable. A liner implosion with an initial launch angle of 45 degrees is shown in Fig. 19. This is accomplished by having both a conical magnet and

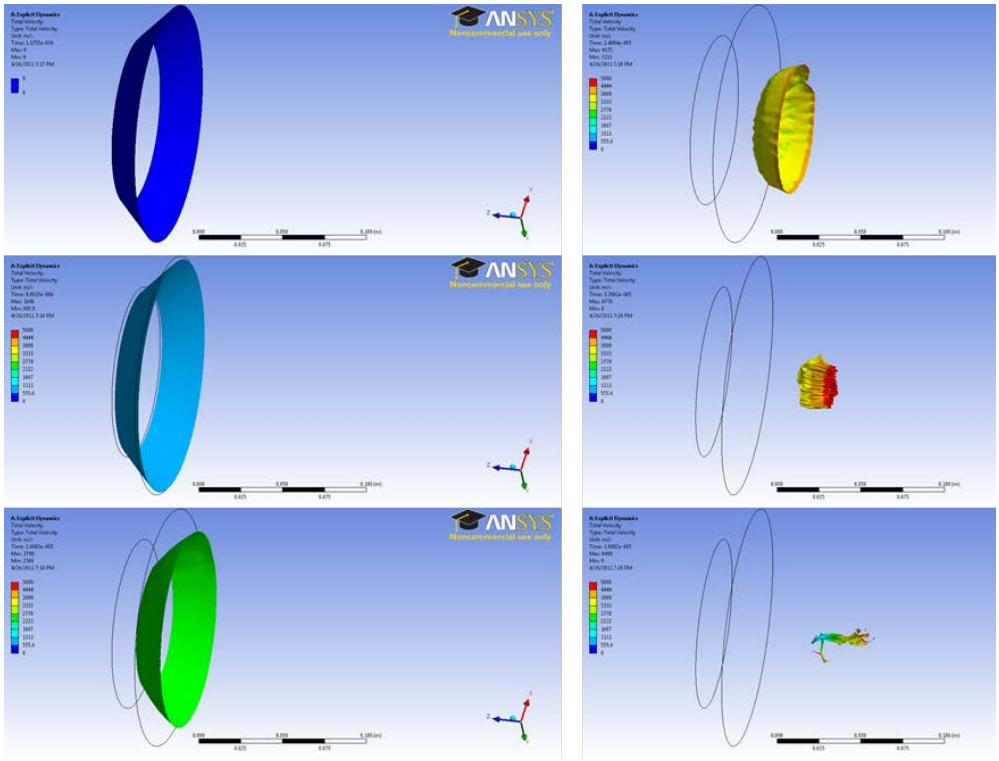

Figure 19. Figure 14. R-Z launch of a 4 mil Aluminum liner with a 15 T peak magnetic field. Times are at 0, 8, 16, 24, 32 and 38 μsec. Color indicates total velocity. Red ⇔ 5 km/s.

conical foil. The foil was imploded with the same 15 T field but with a bit thinner (4 mil) Al liner to keep the implosion time similar to the straight radial implosion.

A calculation for a possible experiment on the scale of the current FLC testbed employing a fully 3D compression is shown in Fig. 20.

Liner Implosion Modeling at the UW

An initial objective of this project was to employ the Mach2 code to model the acceleration and implosion of the foil liner. After installing the official Air Force release version of the code on the PSI-Center's ICE cluster, it was found that it did not include the θ-pinch type boundary conditions that had been developed for a different version. These boundary conditions are essential for the foil-liner simulations, and a version of the code that includes this version was located, and simulations were performed.

These simulations include a geometry with a 20cm long aluminum liner with 9cm outer radius, a 20 cm long theta pinch coil with 10cm inner radius and a 40cm long flux conserver with 20cm radius surrounding everything. Symmetry about the z=0 plane is assumed and only the top half is modeled. Liner motion includes elastoplastic flow and all material

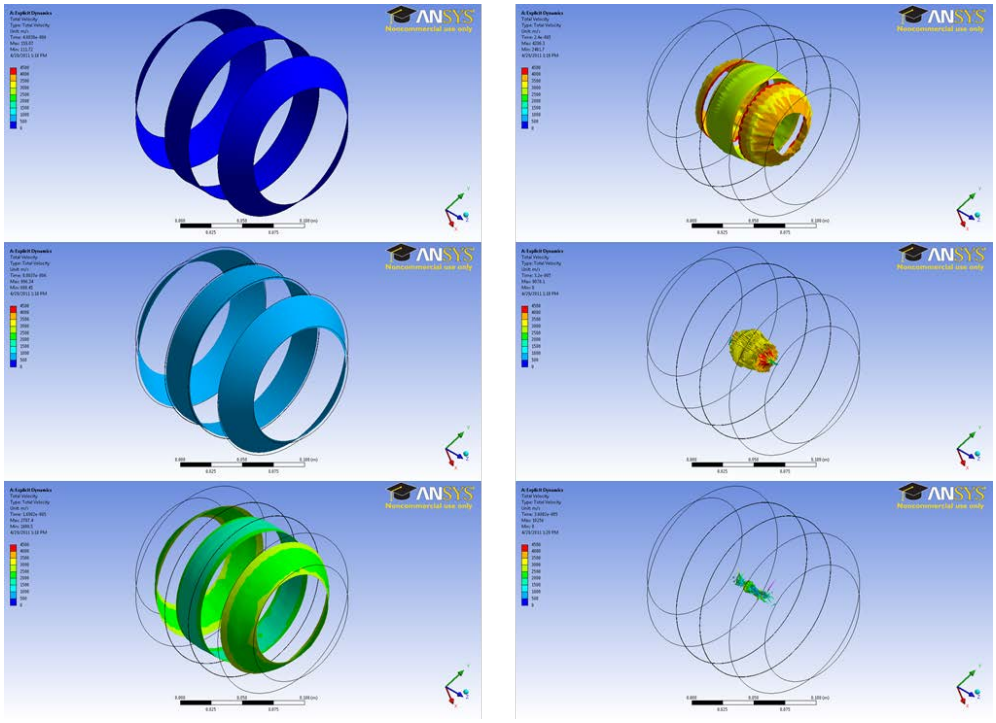

Figure 20. 3D compression employing three 4 mil Aluminum liners each driven with a 15 T peak magnetic field. Times are at 0, 8, 16, 24, 32 and 36 μsec. Color indicates radial velocity. Red ⇔ 5 km/s.

properties are taken from the Sesame library. The material outside the liner is low density, low temperature neutral hydrogen with very high resistivity. The coil is 2 cm thick and the voltage is fixed at 25 kV, making the flux ramp up linearly from an initial value of zero. The goal for the liner thickness is 0.12 mm but most runs use 1 cm and a few use 1 mm. The code is run in both Lagrangian mode with adaptive mesh and in Eulerian mode with material interface tracking. The geometry is illustrated in Figure 21. In this figure the liner is colored, and field lines (brown lines) are seen to be compressed between the coil and the liner.

Initial calculations were run using a pure Lagrangian computational mesh, using an artificially thick liner of 1 cm and 1 mm. In all cases the liner does not move very far before grid crossing occurs, which terminates the simulation. However, prior to termination an important feature of the liner motion can already be seen: the tendency of the end of the liner to curl inward. Then an attempt was made to run the simulations using an adaptive mesh. The first attempt to make the mesh adapt used Mach2's native Brackbill-Saltzman mesh generator. Dozens of runs were made with different settings but they all failed as the mesh became tangled at the liner end. Two different methods of adapting the mesh were written into the code but made little improvement. The first used a simple proportional

scaling to adjust the cell sizes to the liner position. This method did not make the mesh curl inward with the liner. The other method solved a Laplace equation for the grid velocity with the liner velocity as a boundary condition. This was numerically unstable but with smoothing, achieved a .63 radial compression before the mesh again became too tangled at the liner end.

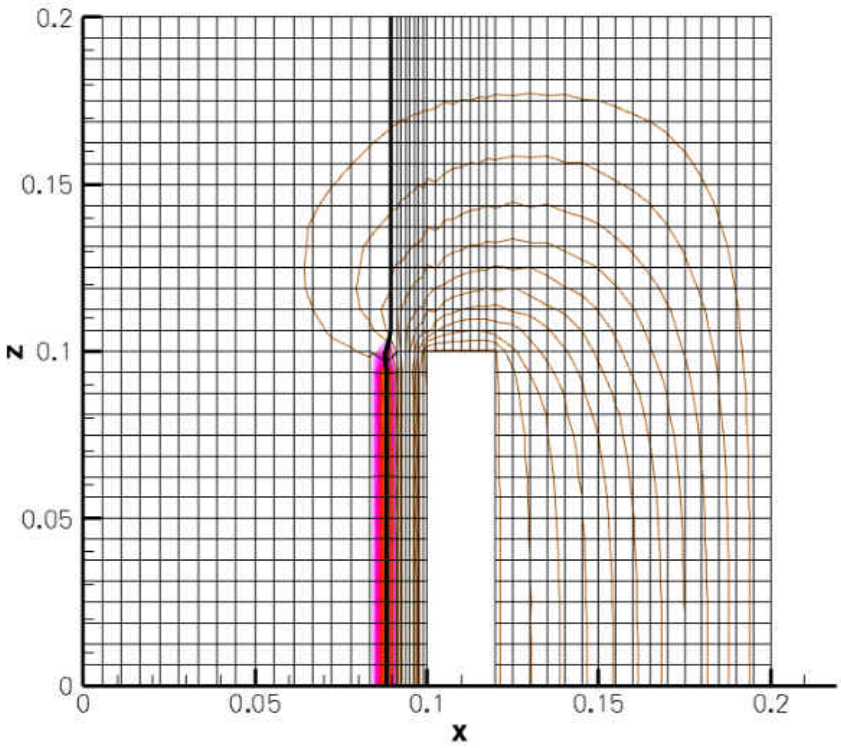

Figure 21. Illustration of geometry and grid for Mach2 simulations.

With these discouraging results, an attempt was made to use Mach's interface tracking option with an Eulerian mesh. These calculations will run, but consume approximately ten times more computer time than Lagrangian calculations with the same mesh size. However a much finer mesh is required to achieve the required resolution. As the liner moves out of its initial high resolution region onto the low resolution part of the mesh, all internal profile information is lost and the flux diffusion rate or Ohmic heating rate, for example, loses all accuracy. The only way to maintain accuracy would be to use high resolution everywhere and spend years on each run, or make the mesh adapt, moving the high resolution region with the liner, but that would lead to all the same difficulties that were encountered in the Lagrangian runs.

In view of these pessimistic results it appears unlikely that Mach2 can be adapted to handle this problem with the resources and time allocated to this project. A significant effort into improving the flexibility of the adaptive mesh software would be required, and even then positive results are not guaranteed. The basic problem comes from the structured mesh and the topological constraints that dictate on how the cells have to connect together. One

way around this is to use a code with an unstructured mesh, preferably unstructured triangles, which can easily adapt to any changing geometry. One option is to use a commercial code, such as COMSOL Multiphysics, which employs this type of mesh and is easy to set up with any geometry.

COMSOL Liner Implosion Modeling

Due to the many difficulties encountered with Mach2 modeling of the implosion a thin-liner that is inductively driven by a θ-pinch, a decision was made to develop a new model using the commercial COMSOL Multiphysics package. The problem geometry is a 20 cm long aluminum liner with 10cm inner radius and 0.12 mm thickness, a 20 cm long theta

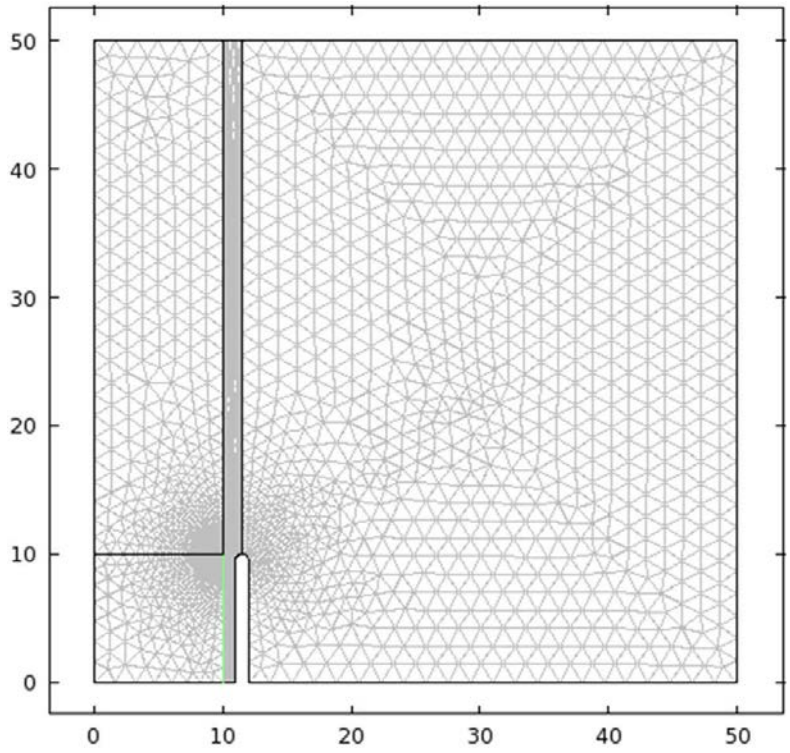

Figure 2. Geometry and mesh used for COMSOL simulations.

pinch coil with 11 cm inner radius and 1 cm thickness, and a 1 m long flux conserver with 50 cm radius surrounding everything. Symmetry about the z = 0 midplane is assumed and only the top half is modeled.

The geometry and mesh are shown in Figure 22. The foil liner, barely visible, is highlighted in green. There are two guidelines attached to the end of the liner, one vertical and one horizontal, and one attached to the end of the coil. They do not represent any physical objects. They divide the mesh into four different zones that move with the liner and guide the mesh motion. The two zones between the liner and the z axis compress radially as the liner implodes. The zone outside the coil remains fixed, and the zone between the liner and

the coil has a mesh that is initially compressed in the radial direction and expands as the liner moves inward. The resolution of the mesh increases locally near the end of the liner where it is needed. Figure 23 shows a blowup of this region. A better solution to the problem of adapting the mesh may be to fully re-mesh the entire domain rather than trying to guide the motion of a deforming mesh. COMSOL has the capability to do this but it is difficult to set up and it has not yet been attempted.

The liner is modeled as an elastic solid with linear isotropic elasticity. The elastic coefficients and the density are obtained from a table of material properties for aluminum at room temperature. The temperature evolution, however, is not included in the present model. Diffusion of magnetic flux into the liner is also not included; the liner is assumed to be perfectly conducting. There is no material outside the liner, just vacuum magnetic field. At the liner-vacuum boundary, the normal component of the elastic stress is required to match the magnetic field pressure. The coil voltage is fixed, usually at 25kV, making the flux ramp up linearly from an initial value of zero. The liner motion is Lagrangian with a moving adaptive mesh outside, as described above.

Several COMSOL simulations have been performed where the coil length is varied. In all cases (so far) the simulations terminate when the grid distortion becomes too large, however by this time the foil has already moved at least half way in and some interesting physics is being revealed. Also, at this time it appears that the grid distortion problem can be resolved with a modest effort, either by judiciously adding more guide-lines, or if

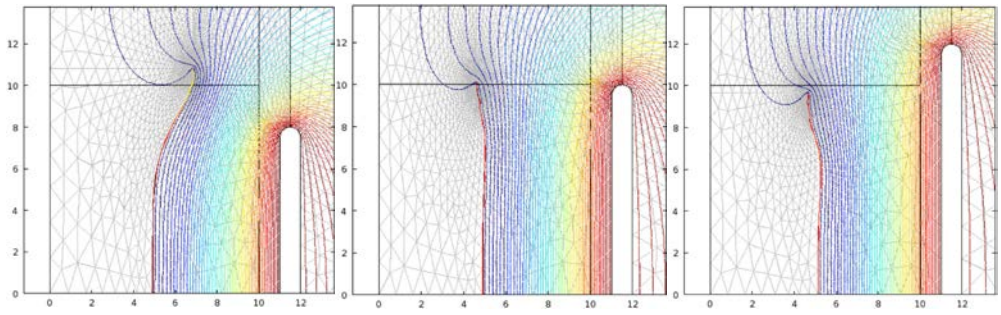

Figure 24. Images of the foil liner, magnetic field-lines, and grid near the termination time for 3 simulations with a coil length of 16 cm (left), 20 cm (center), and 24 cm (right).

necessary employing the COMSOL option to fully re-mesh the entire domain. Figure 24 shows images of the foil liner, magnetic field-lines, and grid near the termination time for 3 simulations with a coil length of 16 cm (left), 20 cm (center), and 24 cm (right). When the coil is shorter than the liner, the center of the liner moves in faster and the liner expands out at the ends, but the axially inward force exerted by the magnetic field cause the liner to curl near the ends. For the case where the liner and the coil are the same length the liner bends inward at the ends and is developing a kink. In the simulation with the longer coil the liner bends inward more near the end due to the increased effect of the magnetic field tension from the lines that wrap around the end of the liner.

It is noted that these simulations were run assuming an elastic solid with a linear isotropic elasticity. In fact the yield stress for aluminum is about 2×10^8 Pa. a value that is exceeded in all of the simulations. When the stress exceeds the yield stress, the linear elastic model is no longer valid so the model will have to be upgraded to use the non-linear elasto-plastic material model which is available in COMSOL's structural mechanics module.

V. DISCUSSION

The successful development of the 3D liner compression of the FRC will validate liner compression as a practical approach to achieving a small scale, low yield source of fusion energy. At a minimum, this method will facilitate the exploration and development of a new regime of fusion plasma physics that could lead to very different application and usage to that now being pursued by virtually all other fusion efforts. At a gain ~ 1-5 there would be application to the breeding of fissile fuel, particularly for the Thorium cycle, to support the future generation of advanced fission plants. There would also be application to the burning and transmuting of long-lived fission products and actinides from commercial fission.

The use of such the IDLC system for space propulsion is now being investigated at MSNW with a grant from NASA. The project represents a unique opportunity to gain the interest of a community that has the resources to rapidly develop the science and technology if the concept can be validated.

For the more ambitious goals of a high efficiency fusion power plant employing direct conversion or a fusion driven rocket, higher fusion gains (10 – 30) are desired. To achieve ignition, a fusion gain $G > 5$, along with sufficient magnetic field for the magnetic confinement of the fusion product alpha (^{4}He) within the FRC plasmoid will be needed. With fusion alpha heating, ignition conditions are achieved and the effective gain can be significantly increased, potentially to as large as several hundred. The necessary magnetic confinement is readily achieved in the compressed FRC plasmoid for the baseline parameters anticipated for the IDLC. While the scale of the validation test is set by the available equipment and energy storage at PDL, better standoff would be achieved by increasing the radius of coil driver for the full scale reactor. Increasing the driver radius by a factor of 2.5 (i.e. a one meter radius liner), the liner mass would also increase by this factor if one were to maintain the same liner velocity and width. This would be sufficient to increase the fusion gain to 6. To achieve a nominal fusion gain of 20, the liner velocity would need to be increased from 2.5 to 4 km/s. With the longer "stroke length" from a larger driver coil, should make this considerably easier to achieve.

ACKNOWLEDGMENTS

The authors wish to gratefully acknowledge the Department of Energy Office of Fusion Energy Sciences and the NASA Institute for Advanced Concepts for support of this work.

REFERENCES

1. R.P. DRAKE, J.H. HAMMER, C.W. HARTMAN, L.J. PERKINS, and D.D. RYUTOV, "Submegajoule liner implosion of a closed field line configuration" *Fusion Technology*, **30**, 310 (1996).

2. M.M. BASKO, A.J. KEMP, J. MEYER-TER-VEHN, "Ignition conditions for magnetized target fusion in cylindrical geometry"**,** *Nuclear Fusion*, **40**, 59 (2000).

3. R.E. SIEMON, I.R. LINDEMUTH, and K.F. SCHOENBERG, "Why MTF is a low cost path to fusion", *Comments Plasma Physics Controlled Fusion* **18**, 363 (1999).

4. J. H. DEGNAN, ET AL. "Compression of Plasma to Megabar Range using Imploding Liner". *Phys. Rev. Lett.*, **82,** 2681(1999).

5. J. SLOUGH, ET AL., "Confinement and Stability of Plasmas in a Field Reversed Configuration", *Phys. Rev. Lett.*, **79**, 2212 (1992).

6. J.T. SLOUGH, ET AL., "Transport, energy balance, and stability of a large field-reversed configuration", *Physics of Plasmas* **2,** 2286 (1995).

7. G. VOTROUBEK, J. SLOUGH, S. ANDREASON, and C. PIHL, "Formation of a Stable Field Reversed Configuration through Merging" *J. Fusion Energy* **27**, 123 (2008).

8. JOHN SLOUGH, GEORGE VOTROUBEK and CHRIS PIHL, "Creation of a high-temperature plasma through merging and compression of supersonic field reversed configuration plasmoids", *Nuclear Fusion*, **51**, 053008 (2011).

9. M.W. BINDERBAUER, ET AL., *Phys. Rev. Lett*., **105**, 045003 (2010).

10. J.T. SLOUGH and K.E. MILLER, "Enhanced Confinement and Stability of a Field Reversed Configuration with Rotating Magnetic Field Current Drive", *Phys. Rev. Lett.*, **85** 1444, (2000).

11. ANTHONY PANCOTTI, JOHN T. SLOUGH, DAVID KIRTLEY, MICHAEL PFAFF, CHRISTOPHER PIHL, GEORGE VOTROUBEK, "Mission Design Architecture for the Fusion Driven Rocket", *AIAA Joint Propulsion Conference 2012*, Atlanta, GA, Control ID: 1286040.

12. E.C. CNARE, "Magnetic Flux Compression by Magnetically Imploded Metallic Foils", *Journal of Applied Physics*, Vol. 27, No. 10, pg. 3812, (1967).

13. Y. H. MATSUDA, F. HERLACH, S. IKEDA, and N. MIURA, "Generation of 600 T by electromagnetic flux compression with improved implosion symmetry"**,** *Rev. Sci. Instrum***. 73** 4288 (2002).

14. T.A. OLIPHANT, F.L. RIBE, and T.A. COULTAS, "Direct Conversion of Thermonuclear Plasma energy by High Magnetic Compression and expansion", *Nuclear Fusion* **13**, 529 (1973).

15. JOHN SLOUGH, SAMUEL ANDREASON, HIROSHI GOTA, CHRIS PIHL, and GEORGE VOTROUBEK, “The Pulsed High Density Experiment: Concept, Design, and Initial Results”, *J. of Fusion Energy*, **25**, (2006)

16. G. VOTROUBEK and J. SLOUGH, “The Plasma Liner Compression Experiment”, *J. of Fusion Energy* **29**, 571 (2010).